UNIVERSITY OF OKLAHOMA

GRADUATE COLLEGE

IMPORTANCE OF PORE SIZE FOR EFFECTIVE DENSITY OF SHALE GAS

A THESIS

SUBMITTED TO THE GRADUATE FACULTY

in partial fulfillment of the requirements for the

Degree of

MASTER OF SCIENCE

By

JAMES GREGORY CURTIN III
Norman, Oklahoma
2017

IMPORTANCE OF PORE SIZE FOR EFFECTIVE DENSITY OF SHALE GAS

A THESIS APPROVED FOR THE
MEWBOURNE SCHOOL OF PETROLEUM AND GEOLOGICAL
ENGINEERING

BY

_____
Dr. Ahmad Sakhaee-Pour, Chair

_____
Dr. Mashhad Fahes

_____
Dr. Xingru Wu

I dedicate this thesis to my loving wife Cheryl, without whom my continued education and this thesis would not have been possible.

Acknowledgements

I would like to first acknowledge the significant guidance and assistance I received from my adviser, Dr. Ahmad Sakhaee-Pour. Dr. Sakhaee-Pour pushed me to ask the right questions and to draw the logical conclusion throughout my thesis process.

I would also like to acknowledge the faculty and staff of the University of Oklahoma Mewbourne School of Petroleum and Geological Engineering and Graduate College. All were supportive and helpful, even when I was late meeting paperwork deadlines.

Finally, I would like to acknowledge my fellow graduate students in the Mewbourne School of Petroleum and Geological Engineering. They have formed a mutually supportive community that helped throughout my graduate school experience in innumerable small ways.

Table of Contents

List of Tables

List of Figures

Abstract

The proper development of any natural gas reservoir depends on knowing several key factors; perhaps the most important of these factors is the volume of gas-in-place of a reservoir at a given pressure. Gas-in-place calculations determine the economic value of gas reserves and tell us whether and how they can be economically developed. Accurately determining gas-in-place and ultimate gas recovery require accurate fluid density data.

This thesis demonstrates the importance of a pore size for fluid densities in shale formations. The fluid density increase significantly for pores whose diameters are smaller than 10 nm. However, what is equally significant is the pore size distribution of the rock tested and whether that distribution represents pore-body sizes or pore-throat sizes. For two Barnett shale samples used in this thesis, it was found that the effect of pore-body size on effective gas density is insignificant at pressures consistent with formation depth when calculating gas-in-place. This conclusion is reached assuming that the pore-body size distribution, not the pore-throat size distribution, best characterizes the pore geometry when calculating gas in place

The numerical results of this theses are only valid for the samples with similar pore-body size distributions. However, they have important qualitative implications for reservoir simulation and production. Simulations that calculate gas density based on pore-throat size distribution, as opposed to pore-body size distribution, will produce higher effective gas density than the in-situ value; thus, they lead to an overly optimistic hydrocarbon in-place and ultimate recovery estimates. As the effective density is a key

component for viscosity and phase behavior of petroleum resources production estimates generated by these models will also be unrealistic.

Chapter 1: Introduction

1.1.Problem statement

The proper development of any natural gas reservoir depends on knowing several key factors; perhaps the most important of these factors is the volume of gas-in-place at any point during the production of a reservoir. Gas-in-place calculations determine the economic value of gas reserves for all formation types and are used to determine if a reservoir can be economically developed as well as how the field should be produced if developed.

For conventional reservoirs, gas-in-place values are calculated using one of three methods: volumetric methods, material-balance methods, or decline-curve-analysis methods. Volumetric methods calculate gas-in-place as a function of pore space available to gas and an equation of state that calculates gas density as a function of pressure and temperature. Material-balance methods make use of early production data but still treat gas volume and density as a function of pressure and temperature. Decline-curve-analysis methods assumes that future production will be similar to past production, but they are affected by well stimulation and less than optimal production. These methods may produce values within an acceptable range of error for conventional reservoirs.

The expansion of natural gas production into tight sand and shale formations has been made economically viable with the development of hydraulic fracturing and horizontal drilling technologies. According to the U.S. Energy Information Administration, shale gas production accounted for only ten percent of all natural gas

produced in the U.S. in 2003, but reached more than 50% in 2015 and is expected to reach approximately 70% by 2040 (EIA, 2017). However, with the expansion of gas production into tight formations the accuracy of traditional gas-in-place calculations have been brought into question. Material-balance methods only work in single-phase gas reservoirs over limited pressure ranges, and the significant production and injection of water as well as geomechanical effects and multi-well production effects result in significant errors in shale gas-in-place calculations (Shahamat and Clarkson, 2017). Decline-curve-analysis methods have been found to produce over-optimistic results when applied to shale formations due to the use of physically unrealistic exponent values used to force curve fit (Denney, 2012).

Volumetric methods use equations of state to calculate gas-in-place that do not account for the influence of the pore walls on the density of the gas contained within those pores. However, the density of natural gas increases significantly near pore walls due to attractive forces between the fluid molecules and the pore wall, regardless of pore size. This phenomenon is ignored in most equations of state as the fraction of gas near the pore wall is assumed to be insignificant when compared to the total pore volume. Danesh (1998) showed that for pores with diameters less than 10 nm wide, the difference between the actual density of gas contained and the amount calculated by traditional equations of state is significant. Unfortunately, in tight sand and shale formations the pore sizes are in the nanoscale making that assumption no longer valid. As a significant percentage of the total pore volume in shales is contained in pores of less than 10 nm diameter, the effect of pore size on gas-in-place calculations needs to be established.

Unfortunately, the pore sizes of a formation and their corresponding distribution are not always clearly understood. While pore space is often modeled as either a bundle of cylindrical tubes of varying diameters (Purcell, 1949) or as lattice of regular tubes (Fatt, 1956), this is not an accurate depiction of actual pore space. This inaccuracy is more pronounced in shale formations whose pore space has low connectivity and acyclic structure (Sakhaee-Pour and Bryant, 2015). Actual pore space is comprised of relatively wide pore bodies interconnected by narrower pore throats.

Pore bodies comprise the majority of pore volume. As such, they may be determined using adsorption-desorption tests. An adsorption-desorption test uses the volume of adsorbed gas to determine pore-body size and distribution.

Pore throats contribute less pore volume but have a dominate effect on fluid transport through the formation. This is because fluids must pass through the pore throat to advance to the next pore. Pore throat sizes are often calculated using drainage data and capillary pressure calculations.

Uncertainty arises when pore sizes are reported without clear distinction between pore bodies and pore throats. As the pore-throat sizes have a greater impact on gas flow and drainage test such as mercury intrusion can accurately measure pore-throat sizes in the nanometer scale, pore-throat sizes are often reported as pore size data.

The actual change in gas density for these nanopores with respect to unconfined density is not exactly known. Several different approaches have been developed to model fluids in these small pores. Molecular dynamic simulations were used by Ambrose et al. (2012) to model the density distribution of pure methane molecules in slit-shaped graphite pores. Several different local density functions have been proposed,

first by Rangarajan et al. (1995), that determine fluid density as a function or pressure, temperature and distance from a pore wall. Finally, modifications to existing equations of state, such as the van der Waals and Peng-Robinson equations of state, can be used to determine gas volume in confined spaces analytically.

1.2.Objective

This thesis examines the importance pore-body sizes versus pore throat size for effective gas density for shale formations. This is accomplished by using pore-body and pore-throat size distribution data previously collected on two shale samples and a Simplified Local Density function (SLD) to model the gas density for each pore-body and pore-throat size.

In order to determine the impact of small pores on gas volume estimations, an average density for representative pore-body and pore-throat sizes were calculated at given pressures and temperature. The average densities were then applied to the pore-body and pore-throat distribution data to establish an effective density for each sample. This effective density was then compared to density values calculated for unconfined space at the same pressures and temperature to determine the significance of the effect nanopores have on gas-in place-calculations.

Chapter 2: Literature review

This thesis depends on two main points. First is the difference between the pore-body size and pore-throat size distributions in shale gas reservoirs. The second is the effect of nanoscale pore-body size, as opposed to pore-throat size, on the effective density of the gas contained therein. This literature review focuses on publications related to both of these topics.

2.1. Barnett Shale gas reservoir

Shale formations are important rocks for hydrocarbon production. Shales have been seen as both source rocks and seals for conventional reservoirs since the beginning of the petroleum industry. With the recent combination of horizontal drilling and hydraulic fracturing, shale formations are now reservoirs for both oil and gas.

The Barnett Shale is a gas-shale play of the Fort Worth basin. The formation is made up of organic rich, petroliferous black shale formed in the middle to late Mississippian period (Montgomery et al., 2005). The Barnett Shale is the probable source rock for hydrocarbon reservoirs throughout north-central Texas. With its development as a gas play by Mitchell Energy in the 1980s and 1990, the Barnett Shale became a major gas play. The Newark East field, part of the Barnett Shale located in Denton, Tarrant and Wise counties, became the largest gas field in Texas in terms of monthly production from 2000 to 2003. The Newark East field is slightly over-pressured at 0.52 psi/ft., has an average porosity of 6% and has permeabilities ranging from microdarcies up to 0.01 md.

The pore-body and pore-throat size distributions used in this thesis are for Barnett Shale cores from the Mitchell 2 T.P. Sims well in Wise County, Texas. The well, drilled in 1991, is roughly 25 miles northwest of Fort Worth. In this area, the Barnett is divided into upper and lower Barnett intervals, separated by the Forestburg limestone, with an average reservoir pressure of 3800 psi (Hickey and Henk, 2007). The core samples were from a depth of 7610 to 7756 ft. The Barnett at this location is an organic-rich black shale with total organic carbon content larger than 2 to 3%. Hickey and Henk identified six major lithofacies: organic shale at 7679 ft., fossiliferous shale at 7658 ft., concretionary carbonate at 7704 ft., dolomitic rhomb shale at 7714 ft., phosphatic pellet grainstone at 7730 ft. and dolomitic shale at 7751 ft.

2.2. Pore size measurements

Pore size measurements can be divided into two groups, those that effectively measure the volume of the pore bodies in a sample and those that measure the capillary pressure and drainage volume in order to calculate the pore-throat diameters and their corresponding distribution.

2.2.1. Pore-throat size measurements

Mercury intrusion capillary pressure (MICP) is commonly used to study pore size distribution in porous medium. This method works by applying an external pressure to the non-wetting phase mercury to overcome the surface tension preventing mercury's injection into the pores of the sample. The pressure required to enter the pore is inversely proportional to the radius of the pore, and is calculated by use of the Washburn equation:

$$P_c = \frac{2\gamma cos\varphi}{r} \quad (1)$$

where P_c is the capillary pressure, $\gamma$is the surface tension, φ is the contact angle of the liquid on the pore wall, and r is the radius of the pore (Washburn, 1921). This equation assumes that pores are cylindrical and equally accessible from the outer surface of the sample. The pore radius measurements are therefore limited only by the pressure that can be applied to the sample, typically 60,000 psi. By increasing the pressure in a series of steps and measuring the volume of mercury injected at each step, a distribution of pore radii is generated. Mercury intrusion is routinely used to measure pores from 3.6 nm to 360 μm (Webb 2001).

There are however issues with using MICP. First, there is the issue of rock compressibility at the high pressures required to measure the smallest pores. There is also the possibility of breaking the rock particles and accessing closed pore space. Also, accurate pore-body size distributions require all small pores to be accessible by larger pores. Actual pore geometry tends to be made up of larger pore bodies accessed by smaller pore throats. Because the larger pore-body volumes cannot be accessed by the mercury until sufficient pressure is reached to overcome the surface tension of the pore throats, this should limit MCIP to measuring pore-throat size distributions. Errors can and do occur when MCIP data is used for pore-body size distributions. Finally, actual pores are not cylindrical as assumed in the Washburn equation.

2.2.2. Pore-body size measurements

The chemical, ceramic, and pharmaceutical industries commonly use subcritical gas adsorption/desorption test to characterize the pore geometry of microporous materials like activated carbon, carbon nanotubes, zeolites and catalyst. The most

commonly used gas is for this technique is nitrogen; it performs best for substances with dominated by pores between 2 and 50 nm. This technique is unable to measure pores with diameters larger than 200 nm (Kuila and Prasad, 2013).

Nitrogen gas-adsorption works by exposing a degassed sample to nitrogen gas at constant cryogenic liquid nitrogen temperature, -323.14 º F (-197.3 º C) in a series of stepwise increasing pressures. The volume of adsorbed nitrogen is measured at each pressure. The porous media adsorbs gas through several different mechanisms. Micropore filling will occur at low-relative pressures due to interactions between the adsorbent and adsorbate. At slightly greater pressure, mesopores and macropores will start, first as a single molecular layer until the available pore surface is covered and then as a multi-molecular layer. At larger relative pressures the gas begins to condense, at pressures less than the vapor pressure, into a liquid due to capillary condensation. Because gas condensates at different pressures for different pore diameters, a pore size distribution can be created by measuring the amount of gas condensing at each relative pressure. The pore size distribution is found by creating an adsorption isotherm by plotting the volume of adsorbed gas as a function or pressure normalized by the saturated vapor pressure. The sample is then depressurized and the volume of nitrogen outgassed is measured. Also, due to hysteresis between the adsorption and desorption isotherms, pore connectivity can also be examined.

A second method for pore-body size measurements is nuclear magnetic resonance (NMR). NMR can be used to determine a pore-body distribution by measuring the amount of fluid present in the sample porosity at discreet relaxation times. Protons within the pores are magnetized and diffuse throughout the entire pore

before losing their magnetization. The time required for this lose is the T_2 relaxation time and can be used to find pore body size with the following equation:

$$\frac{1}{T_2} = \frac{1}{T_{2\,bulk}} + \rho_2 \frac{s}{v} + D\frac{(\gamma GTE)^2}{12} \quad (2)$$

where $T_{2\,bulk}$ is the bulk relaxation time, ρ_2 is the surface relaxivity, s/v is the pore surface to volume ration, *D* is the bulk diffusion coefficient of the confined fluid, γ is the gyromagnetic ratio, *G* is the magnetic field gradient, and *TE* is the echo spacing time. If the surface relaxivity is known, then the pore-body size distribution can be determined from the T_2 distribution (Tinni et al., 2014).

2.3. Pore space model

The model used to characterize the pore space of a sample is important for analyzing the nitrogen adsorption/desorption data. The simplest model is the bundle-of-tubes model proposed by Purcell (1949). This model consists of series of parallel tubes of various diameters. The advantage of this model is its simplicity and that single-phase permeability can be related to MICP drainage data. Unfortunately, this model does not provide a realistic image of the rock and ignores pore connectivity.

In order to capture the effect of pore interconnectivity, Fatt (1956) proposed a model comprised of interconnected tubes arranged in a two-dimensional square lattice. With this model, residual wetting phase saturations in both drainage and imbibition could be captured. This model works well when used to represent the pore space of conventional petroleum reservoirs, such as unconsolidated sandstones. However, this model also fails to provide a realistic model of pore space.

Bryant et al. (1993) used spheres to represent the grains of a sedimentary rock and the random packing of those sphere to model the rock. The space between the spheres then represents the pore space of the rock. This model space provided an estimate of permeability when subjected to a pressure gradient. Once again, this model worked best for conventional reservoirs.

For this thesis, the pore-body size distribution was created using an acyclic pore model (Zapata and Sakhaee-Pour, 2016). The acyclic pore model features a unique path between any two points in the model. The great advantage to this model is that smaller pores do not restrict access to larger pores; all narrow pores are accessed by larger pore throats. This model overcomes the pore-throat limitation of mercury intrusion. However, this model is limited to samples where the variation of the capillary pressure with the wetting phase saturation has a non-plateau like trend (Sakhaee-Pour and Bryant, 2015). The samples used in this thesis meet this criterion.

2.4. Models of gas density in confined spaces

Currently, there are three common models for calculating gas density in confined spaces. First is molecular simulations that build up a fluid molecule distribution molecule by molecule within a given pore geometry. The second is the density functions that calculate density as a function of pressure, temperature, and distance from a pore wall for the given pore space. The third is modified equations of state that take existing equations of state, such as van der Waals or Peng-Robinson equations of state, and add additional terms to account for fluid molecule-pore wall interactions.

2.4.1. Molecular simulations

Molecular simulations determine the density of gas in a confined space by modeling a single pore with a set number of fluid molecules within the pore. Ambrose et al. (2012) used a molecular dynamics simulation to simulate methane adsorption in slit-shaped pores. The simulation assumed two parallel graphene pore walls set at variable distances apart in the *z* direction. The length of each wall in the *y* direction was held constant but the *x* direction length varied in order to insure roughly the same number of fluid particle were contained in pore each size. The methane molecules were modeled using Lennard-Jones potential to account for interactions between the methane fluid molecules and the carbon pore wall molecules. In order to determine density, the actual number of methane molecules per volume were calculated at set distances away from the pore walls. From this a density profile for each pore size was generated. This simulation predicted adsorbed layer densities of 0.34 g/cm^3 for methane. This value is less than the 0.37 g/cm^3 reported by Haydel and Kobayashi (1967) and the 0.42 by Moavor et al. (2004).

Didar and Akkutla (2013) used Monte Carlo simulations to study the adsorption of gases in model nanopores at various pressures and evaluate critical pressure and temperature changes in confined methane. As with the molecular dynamics simulation above, Lennard-Jones potentials were used for the interactions between the pore wall and fluid molecules. The pore walls were modeled as slit-shape graphite, comprised of three layers of graphene. The system is set up as a two box system with the first box containing bulk fluid and the second box containing the slit-shaped pore. The fluid molecules are chosen randomly and allowed to either displace other molecules in the

same box, transition between boxes, or rotate around their center of mass. To evaluate the gas adsorption, an Isobaric-Isothermal Gibbs ensemble was used, where the number of particles, total system pressure and temperature where held constant. To measure the changes in critical pressure and temperature, a Canonical Gibbs ensemble was used, where the number of particles, volume and temperature remain constant.

Mosher et al. (2013) used a grand canonical Monte Carlo algorithm to predict adsorption isotherms at pressures and temperatures relevant to coal and shale gas formations. The model was a collection of independent, non-interconnected slit-shaped carbon pores of various widths. Their results showed that methane adsorption was highly sensitive to pore size. As with all simulation based approaches, this algorithm was computationally expensive, requiring 100 million grand canonical Monte Carlo moves during each simulation.

2.4.2. Density functions

Density functions are numerical models that couple equations of state and thermodynamic equilibrium relations. This approach requires less computational intensive than simulation models.

Rangarajan et al. (1995) was the first to use a simplified local density function to model gas adsorption in several different pore wall and fluid type combinations. The model combined fluid-solid interaction potential with the van der Waals equation of state. This function predicted fugacities and densities across a wide range of pore pressures. This model under predicted gas adsorption by as much as 20% at high pressure, but that difference decreased to less than 1% near 1 bar.

Mohammed et al. (2009) used a simplified local density function based on the Peng-Robinson equation of state to model gas adsorption in coalbeds. This equation of state used a modified *a* parameter based adsorption data of different fluids on coal. This model predicted adsorbed gas amounts with and average absolute deviation of 4.1%.

Chareonsuppanimit et al. (2012) compared experimental gas adsorption data obtained for New Albany shale to values predicted by a simplified local density function based on the Peng-Robinson equation of state. This model used the same modified *a* parameter used by Mohammed et al. to calculate the bulk density, and used a modified a parameter based of the fluid molecule distance from the pore wall to calculate the fluid-fluid fugacity (Chen et al., 1997). This model also modified the *b* parameter based on empirical correlations. Five parameters were also regressed to fit the data: surface area, Ai, solid-solid interaction energy, the fluid molecule-wall molecule interaction energy parameter, and slit length. With these modifications they were able to produce adsorption data with an overall average absolute percentage deviation of 12%.

Ma and Jamili (2016) used a simplified local density function based on the Peng-Robinson equation of state to model density profiles instead of adsorption isotherms for hydrocarbon in shales. This model also used slit-shaped pores and the same modified *a* parameter base on position used above. However, instead of predicting adsorption properties of the gas, their model generated density profiles for the contained fluid across the pore width. This method produced good agreement with density profiles predicted by molecular simulation present in literature.

2.4.3. Modified equations of state

The limitation of molecular simulations and density functions is that they come with large computational cost. This computational cost limits the complexity of model for which they can be used. Therefore, to address this issue models that describe the fluid behavior in less detail but still provide fluid properties of adequate detail were developed. Analytical equations of state can model confined fluids with sufficient accuracy so long as only global fluid properties are needed. Analytical equations of state also have the additional benefit that they can be used to describe both confined and bulk fluids.

Schoen and Diestler (1998) used thermodynamic perturbation theory to model a simple fluid confined in slit-shaped pores. They assumed the fluid had constant density across the pore. Using this method, they modified the van der Waals equation of state. They modified the a parameter in the van der Waals equation of state into a_p, a function of distance from the pore wall. Thus, they were able to develop an equation of state with the same temperature and density dependence as the van der Waals but that was also a function of pore radius. This model predicted lower critical temperatures in confined pores and pore condensation over a range of pressures comparable to experimental results. Unfortunately, because of the simplicity of their model fluid this model failed to predict the correct depression of critical temperature or fluid behavior near the critical point.

Additional early work at developing a pore-size dependent equation of state was developed by Zhu, Ni and Lu (1999). Their goal was to model multilayer adsorption in mesopores, especially the affect pore radius had on adsorbed layer thickness. They used

nitrogen adsorption test on MCM-41 samples with wall thicknesses of 1 nm and pore radii of 2 to 5 nm. Using this method, they were able to develop a relationship between condensation vapor pressure, radius of cylindrical pore, and thickness of the adsorbed film in the pores. This research produced an equation to describe of multilayer adsorption in cylindrical mesopores as well as determine the radii of cylindrical pores from adsorption data.

Giaya and Thompson (2002) used similar methodology to Schoen and Diestler to study water contain in two different hydrophobic pores. They created a model that predicted the density of water inside the pores based on the density of the water outside the pores, the pore radius, and the water-molecule-wall molecule attraction. This model was very sensitive to the fluid-fluid and fluid-wall parameters selected and showed that parameter values that were reasonable for global descriptions of water phase behavior may not work in confined conditions.

By treating pressure as a tensor, Zarragoicoechea and Kuz (2002) developed a modified equation of state for a fluid confined in a square pore with infinite length and a width of less than 5 nm. This work assumed that pore walls were inert, thus ignoring fluid-wall interactions. This equation showed agreement with lattice model based numerical simulation in regards to critical temperature shift and capillary condensation. This method did not change the pre-existing van der Waals parameters *a* or *b*. Zarragoicoechea and Kuz (2004) extended this to a van der Waals equation of state with modified *a* and *b* parameters.

Holovko and Dong (2009) used scaled particle theory to develop an analytical equation of state for a confined hard sphere fluid. An initial error in fluid

compressibility of less than 20%, when compared to grand canonical ensemble Monte Carlo simulation results, was further refined with an empirical correction to less than 7.6%.

Travalloni et al. (2010) developed a modified van der Waals equation of state for pure fluids confined in cylindrical pores based on empirical modeling of confined fluid properties. The purpose of this model was to continuously describe the behavior of fluids as a function of pore radius regardless of confinement degree. It used the same modified parameters *a* and *b* for all pore sizes and had good correlation for pure fluid adsorption data and some mixed fluid adsorption data.

Travalloni et al. (2014) later used the same empirical approach to develop a modified Peng-Robinson equation of state. Barbosa et al. (2016) further refined this modified Peng-Robinson equation of state to correlate with molecular simulation data. This modified Peng-Robinson EOS exhibited better results when compared to experimental data of mixed gas adsorption.

Dong et al. (2016) used the Peng-Robinson equation of state, a capillary pressure equation, and adsorption theory to model critical point shift, capillary pressure rise, and adsorption behavior for a fluid confined in nanopores. Their model ignored capillary condensation and Coulombic forces between the fluid molecules and the pore walls.

Chapter 3: Methodology

In order to compare the effect pore-body and pore-throat sizes have on the effective density of gas in shale nanopores, it is necessary to collect data on pore-body and pore-throat diameters for representative pore samples and to determine the average density for each of those pore radii. Data available in literature provided the pore-body and pore-throat data. A Simplified Local Density model, based on the Peng-Robinson equation of state (SLD-PR), was used to calculate average density for pore-body and pore-throat sizes.

3.1. Pore-body and pore-throat size distributions

Pore-body and pore-throat size distributions for two samples of unpreserved Barnett Shale available in literature were used for this thesis. The mercury intrusion capillary pressure measurements and nitrogen adsorption/desorption were conducted by Jaing et al. (2015) and further analysis on pore size distribution was completed by Zapata and Sakhaee-Pour (2016). The samples are organic rich shales from the Mitchell 2 T.P. Sims well in Wise County, Texas, from depths between 7610 to 7756 ft. (Hickey and Henk, 2007).

Jaing et al. (2015) prepared both samples by crushing them into small fragments, between 70 and 125 micrometers, and then drying them for 48 hours at 220 °C. Two grams of each sample were used for mercury intrusion/extrusion testing performed on a Micrometrics AutoPore III with a pressure range from 1 to 60,000 psi. Approximately 0.5 g of each sample were tested in a 3Flex Surface Characterization Analyzer from Micrometrics to produce nitrogen sorption isotherms at 77 K. Mercury intrusion

capillary pressure data was conformance corrected using Comisky's method (Comisky et al. 2011).

Zapata and Sakhaee-Pour (2016) used an acyclic pore model to determine pore-throat and pore-body size distributions, reproduced in Fig. 1 and 2, from the nitrogen adsorption/desorption and mercury intrusion capillary pressure measurements published in Jaing et al. (2015).

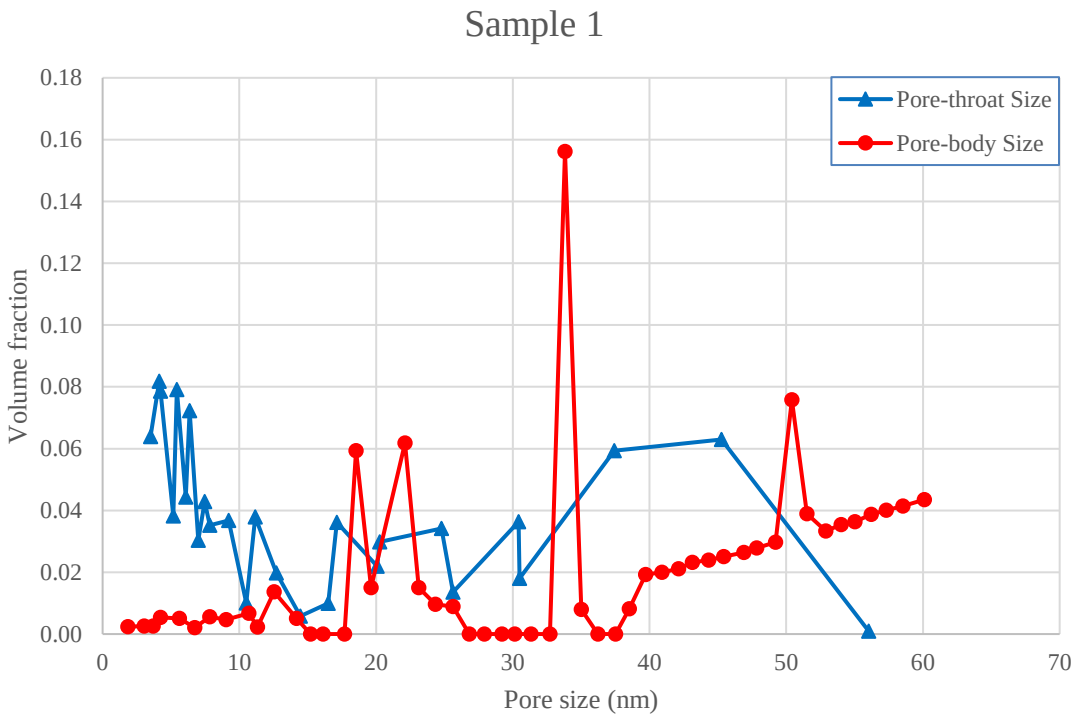

Figure 1: Pore-body and pore-throat distributions for Sample 1.
Pore-body size data was produced using nitrogen adsorption/desorption data and pore-throat size data was produced using mercury intrusion capillary pressure measurements.

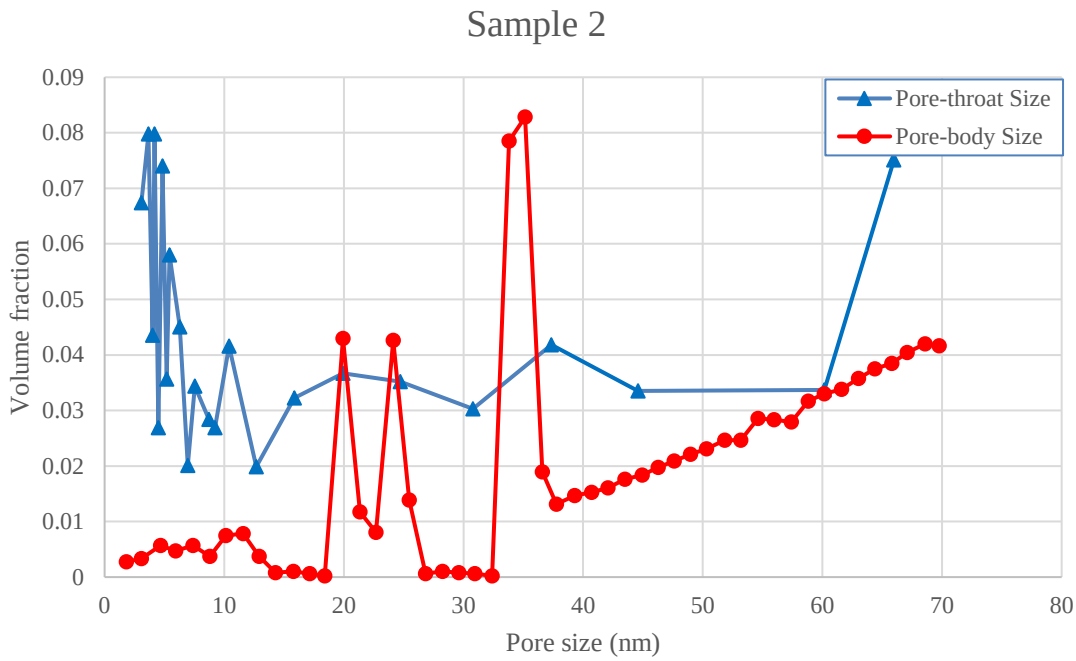

Figure 2: Pore-body and pore-throat distributions for Sample 2.
Pore-body size data was produced using nitrogen adsorption/desorption data and pore-throat size data was produced using mercury intrusion capillary pressure measurements.

3.2. Effective density

The present research uses a Simplified Local Density (SLD) function based on the Peng-Robinson equation of state to determine the average fluid density for each pore size. The particular SLD used in this thesis was proposed by Ma and Jamili (2016) and the full details of the function calculations can be found in their paper. This SLD assumes a slit shape pore profile and produces a fluid density profile across for a given fluid pressure, fluid composition, temperature and pore size. With the fluid pressure, P, composition, temperature, T, and pore size, L, has been selected, a position relative to the pore wall, z, is selected. The fluid-solid chemical potential for both walls, $\mu_{fs}(z)$, at that position is then calculated:

$$\mu_{fs}(z) = N_A \Psi^{fs}(z) \tag{3}$$

Where N_A is Avogadro's number and $\Psi^{fs}(z)$ is the fluid molecule-wall molecule potential energy function. Lee's partially integrated 10-4 Lennard-Jones potential model (Lee 1988) was used to calculate $\Psi^{fs}(z)$:

$$\Psi^{fs}(z) = 4\pi\rho_{atoms}\varepsilon_{fs}\sigma_{fs}^2\left(\frac{\sigma_{fs}^{10}}{5(z')^{10}} - \frac{1}{2}\sum_{i=1}^{4}\frac{\sigma_{fs}^4}{(z'+(i+1)\sigma_{ss})^4}\right) \tag{4}$$

The unconfined fluid density is calculated using the Peng-Robinson equation of state.

$$\frac{P}{\rho RT} = \frac{1}{(1-\rho b)} - \frac{a\rho}{RT\left[1+\left(1-\sqrt{2}\right)\rho b\right]\left[1+\left(1+\sqrt{2}\right)\rho b\right.} \tag{5}$$

Using the unconfined fluid density, the bulk fugacity, f_{bulk}, is then calculated.

$$ln\frac{f_{bulk}}{P} = \frac{b\rho_{bulk}}{1-b\rho_{bulk}} - \frac{a\rho_{bulk}}{RT\left(1+2b\rho_{bulk}-b^2\rho_{bulk}^2\right)} - \ln\left[\frac{P}{RT\rho_{bulk}} - \frac{Pb}{RT}\right] - \frac{a}{2\sqrt{2}bRT}\ \text{x}\ ln\left[\frac{1+(1+\sqrt{2}\rho_{bulk}b}{1+(1-\sqrt{2}\rho_{bulk}b}\right] \tag{6}$$

Then the fluid-fluid fugacity is calculated for the selected position.

$$f_{ff}(z) = f_{bulk}exp\left(-\frac{\mu_{fs1}(z)+\mu_{fs2}(L-z)}{RT}\right) \tag{7}$$

Finally, the density at the selected position is calculated using the Peng-Robinson EOS in terms of fluid-fluid fugacity.

$$ln\frac{f_{ff}}{P} = \frac{b\rho_{local}(z)}{1-b\rho_{local(z)}} - \frac{a_{ff(z)}\rho_{local}(z)}{RT\left(1+2b\rho_{local}(z)-b^2\rho_{local}^2(z)\right)} - \ln\left[\frac{P}{RT\rho_{local}(z)} - \frac{Pb}{RT}\right] - \frac{a_{ff}(z)}{2\sqrt{2}bRT}\ \text{x}\ ln\left[\frac{1+(1+\sqrt{2}\rho_{local}(z)b}{1+(1-\sqrt{2}\rho_{local}(z)b}\right] \tag{8}$$

Then the next position is selected and the process repeated until the local density for all positions have been calculated and a density profile for the entire pore created. A full list of variables used is located in **Table 1**.

Table 1: List of variables used in SLD-PR model.
The ε_{fs} and σ_{fs} values are for methane in a graphite pore. The ρ_{atoms} value is for graphite and the σ_{ss} value is for methane.

Symbol	Definition	Units	Assumed or constant values
a	Attraction parameter	m^6Pa/mol^2	
a_{ff}	Attraction parameter modified for pore position	m^6Pa/mol^2	
b	Repulsion parameter	m^3/mol	
f_{bulk}	Bulk fugacity	Pa	
f_{ff}	Fluid-fluid fugacity	Pa	
k	Boltzmann constant	m^2kg/s^2K	$1.38064852x10^{-23}$
L	Pore width	m	
N_A	Avogadro's number	atoms/mol	$6.0221409x10^{23}$
P	Pressure	Pa	
R	Universal gas constant	$m^3Pa/mol*K$	8.314
T	Temperature	K	
z	Position in pore	m	
ε_{fs}	Fluid molecule-wall molecule interaction energy parameter	K	148.6*k
μ_{fs}	Fluid-solid chemical potential	$atoms^2m^2kg/s^2mol$	
ρ	Density	mol/m^3	
ρ_{atoms}	Number of carbon plane atoms per unit area	$atoms/m^2$	$38.2x10^{-18}$
ρ_{bulk}	Bulk density	mol/m^3	
ρ_{local}	Local density at position z from wall	mol/m^3	
σ_{fs}	Van der Waals molecular diameter	m	$0.355x10^{-9}$
σ_{ss}	Carbon interplaner distance	m	$0.34x10^{-9}$
Ψ_{fs}	Fluid molecule-wall molecule potential energy	$atoms*m^2kg/s^2$	

Using the software application Matlab, the SLD function generated density profiles for several pore widths ranging from 1.81 to 10.82 nm at pressures of 1,000 psia, 2,000 psia, 3,000 psia and 4,000 psia. The modeled fluid was pure methane at 185 °F. A complete density profile was not necessary for this thesis, so the density profiles

for each pore between 1.81 and 10.82 nm were averaged using a weighted average based on volume. Pores with diameters greater than 10.82 nm were assumed to have densities similar to the bulk or unconfined density.

The average density for each pore size calculated above, for pores less than 10.82 nm, was applied to the pore distributions of Samples 1 and 2. Pores larger than or equal to 10.82 nm were assigned the unconfined density. From this an effective density for each sample was obtained.

Chapter 4: Results

In this research, average densities for Samples 1 and 2 were calculated for pores ranging from 1.81 to 10.82 nm at four different pressures: 1000, 2000, 3000 and 4000 psia, and a constant temperature of 185°F. These average densities were then normalized by the unconfined density and plotted in **Fig. 3** and **Fig. 4**. The plots clearly demonstrate the relationship of density to pore size; the average density of each pore increases as the pore size decreases. The effect of pore size on density is also more pronounced at lower pressures than higher ones. For Sample 2, the density of a 1.81 nm diameter pore was more than 3.58 times that of the unconfined density at 1,000 psia, but only 1.56 times that of the bulk density at 4,000 psia.

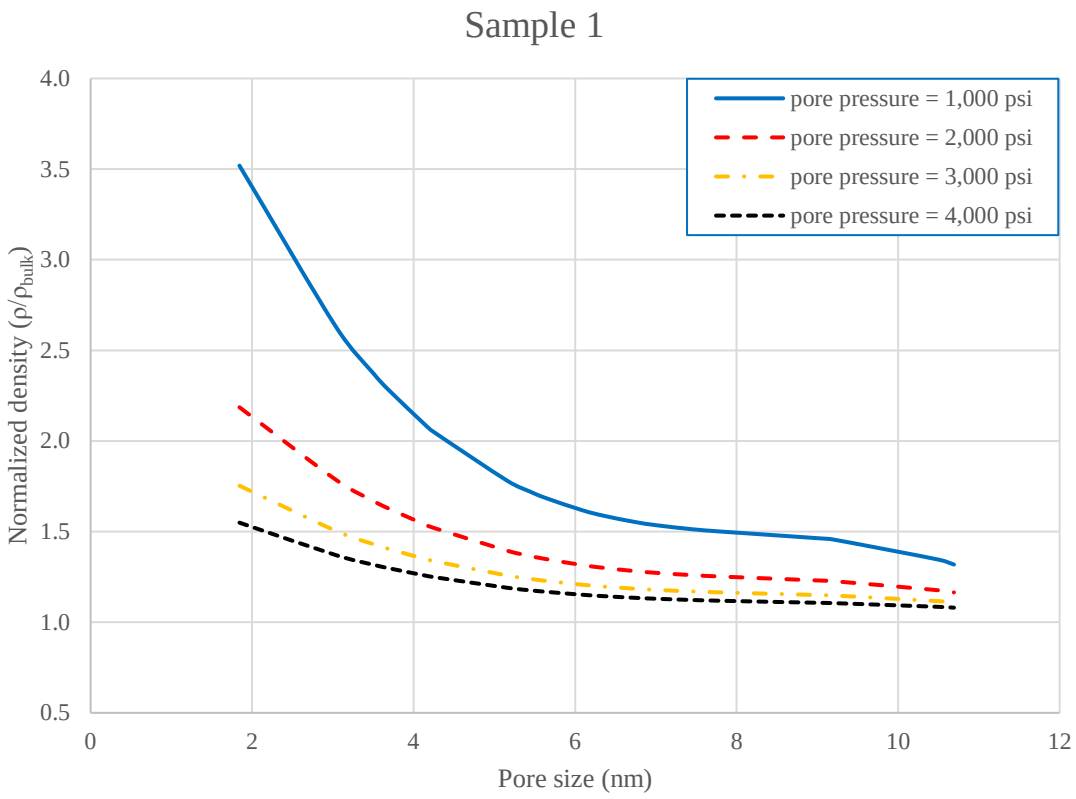

Figure 3. Normalized density versus pore size for Sample 1.

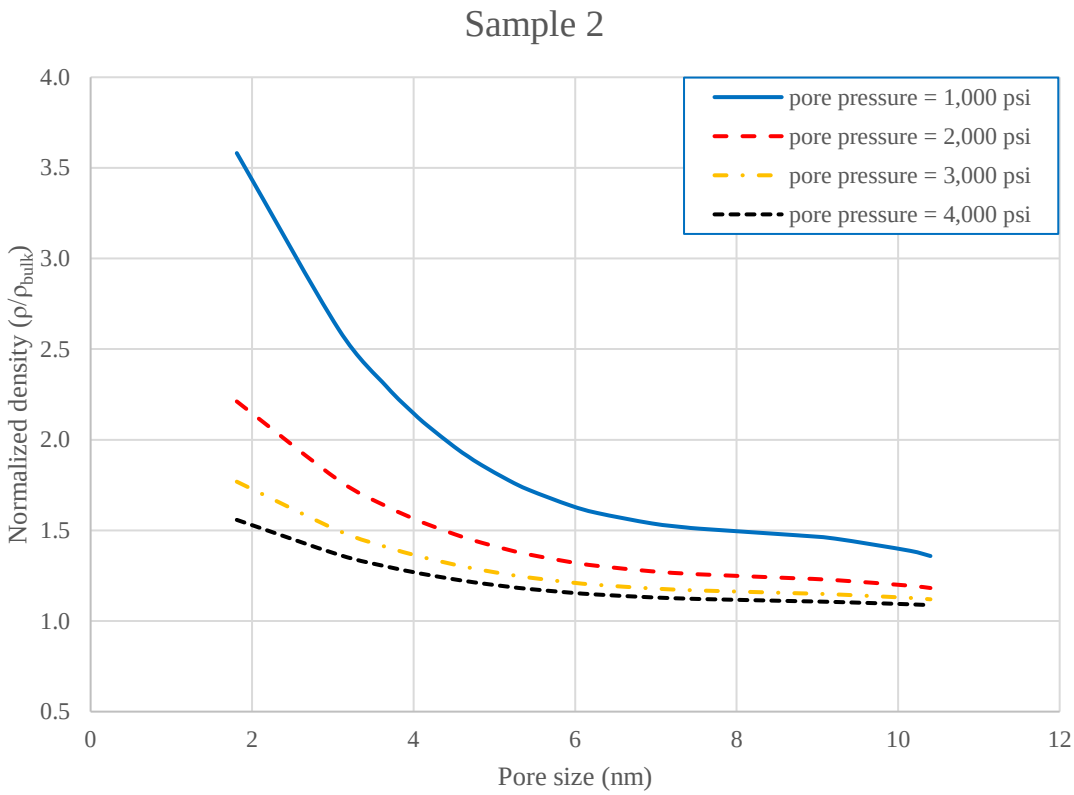

Figure 4: Normalized density versus pore size for Sample 2.

Also, as suggested by prior publications, the effect of pore size on density becomes insignificant as pore sizes increase over 10 nm. For the largest pore tested on Sample 1, a 10.69 nm pore, the fluid density was only 1.36 times that of the unconfined density at 1,000 psia and only 1.09 times that of the unconfined density at 4,000 psia.

The average densities for each pore size were applied to the pore-body and pore-throat size distributions for Sample1 and Sample 2. In both cases the influence of the small pore sizes increased the effective density of methane for each sample. See **Fig. 5** and **Fig. 6**. However, while the increase in effective density for the pore-throat size distribution was significant when compared to bulk values, the pore-body size distribution produced a much more modest increase.

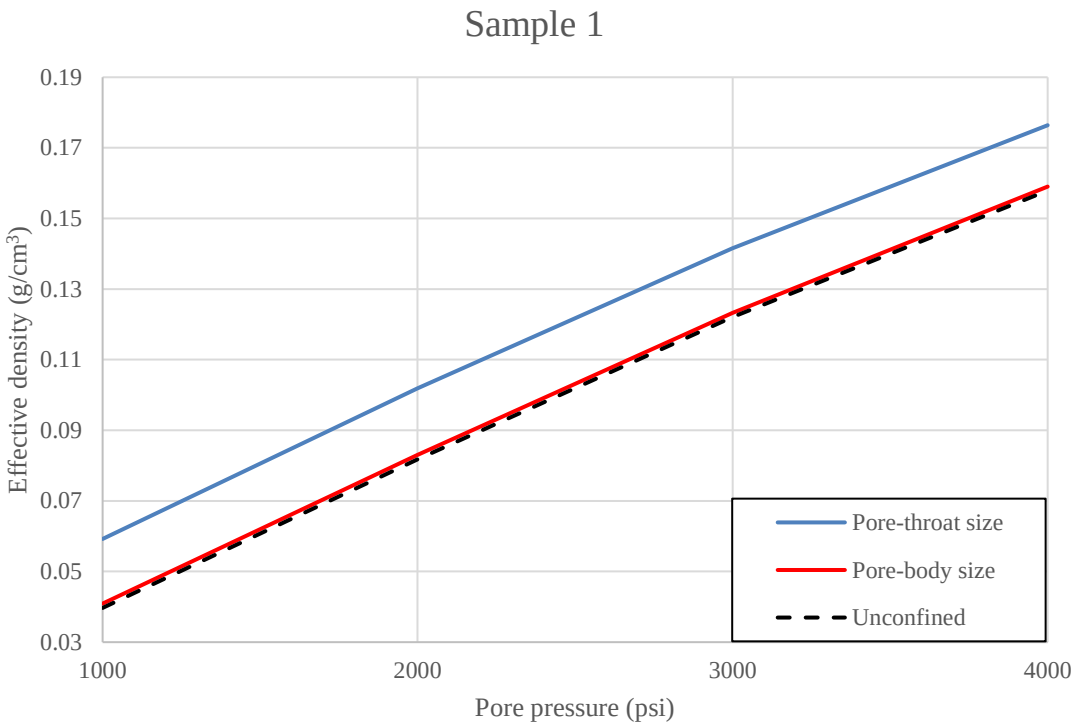

Figure 5: Effective density versus pore pressure for Sample 1.

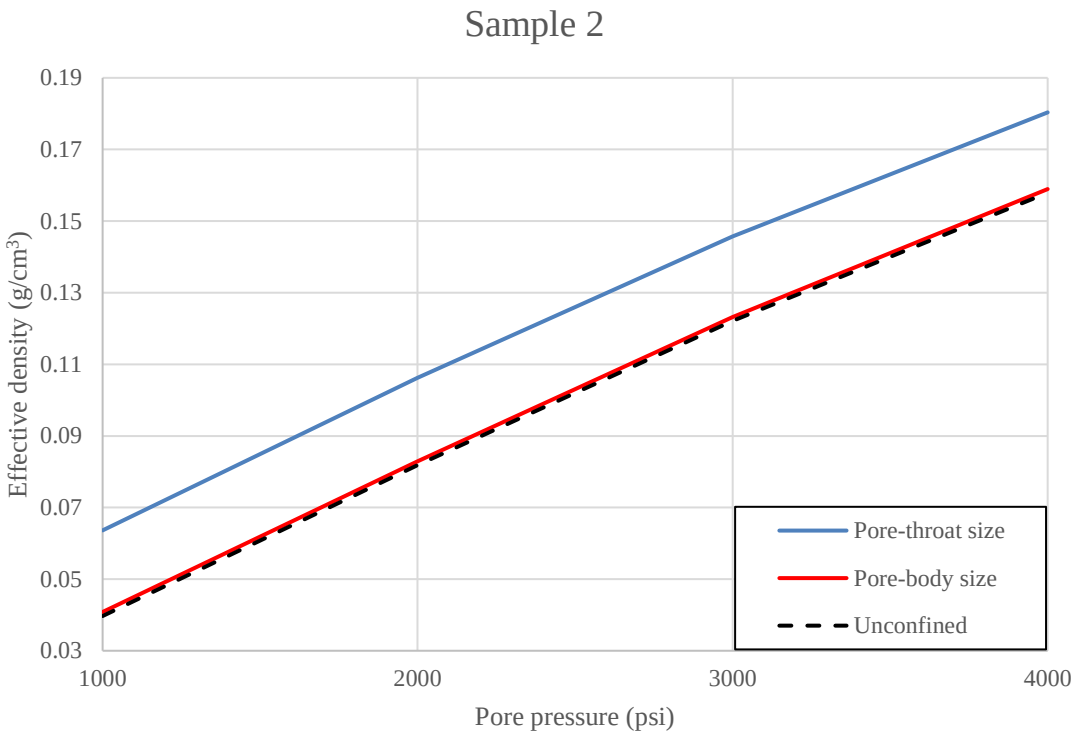

Figure 6: Effective density versus pore pressure for Sample 2.

The full impact of pore-throat versus pore-body size selection was calculated as a deviation percentage. In **Fig. 7** and **Fig. 8** Deviation 1 is defined as the difference in effective density for the pore-body size distribution compared to the unconfined density and Deviation 2 is the difference in effective density compared to the bulk density. For Sample 1 the pore-throat size distribution produced a deviation percentage from 10.9 to 44.7% depending on pressure. The pore-body size distribution only produced a deviation percentage from 0.7 to 3.1% depending on pressure. Similar results were found for Sample 2. The deviation percentage for the pore-body size distribution was between 0.7 to 2.8% and the deviation percentage for the pore-throat size distribution was 13.5 to 55.8%.

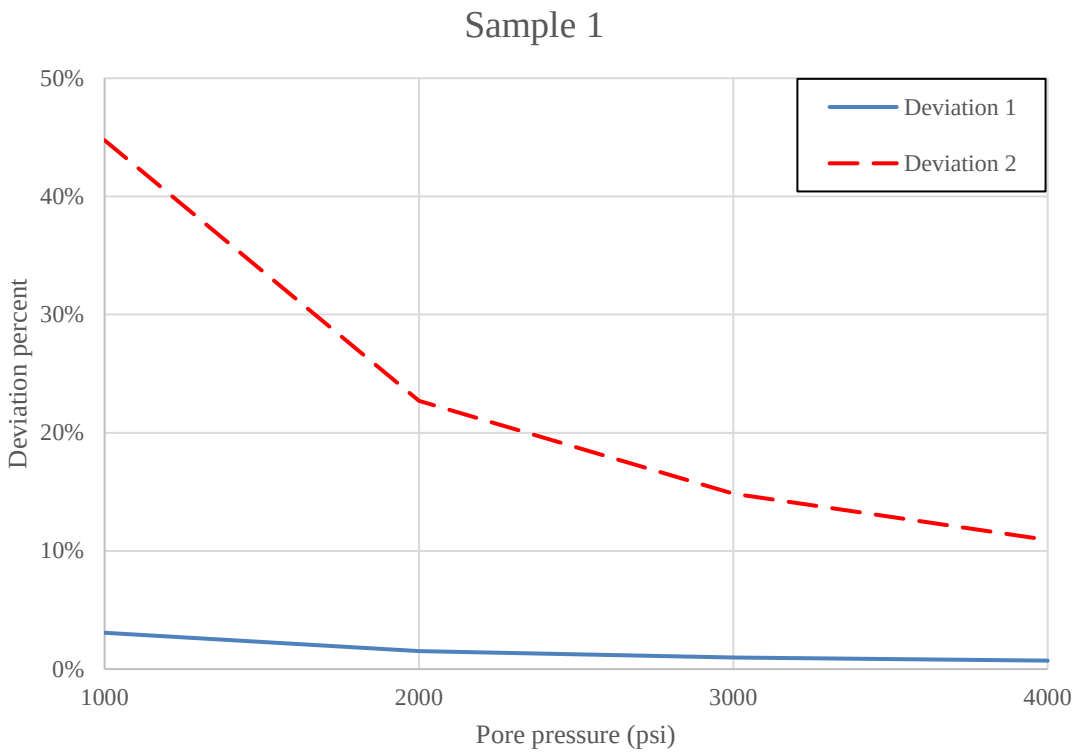

Figure 7: Sample 1 deviation percentage versus pore pressure.

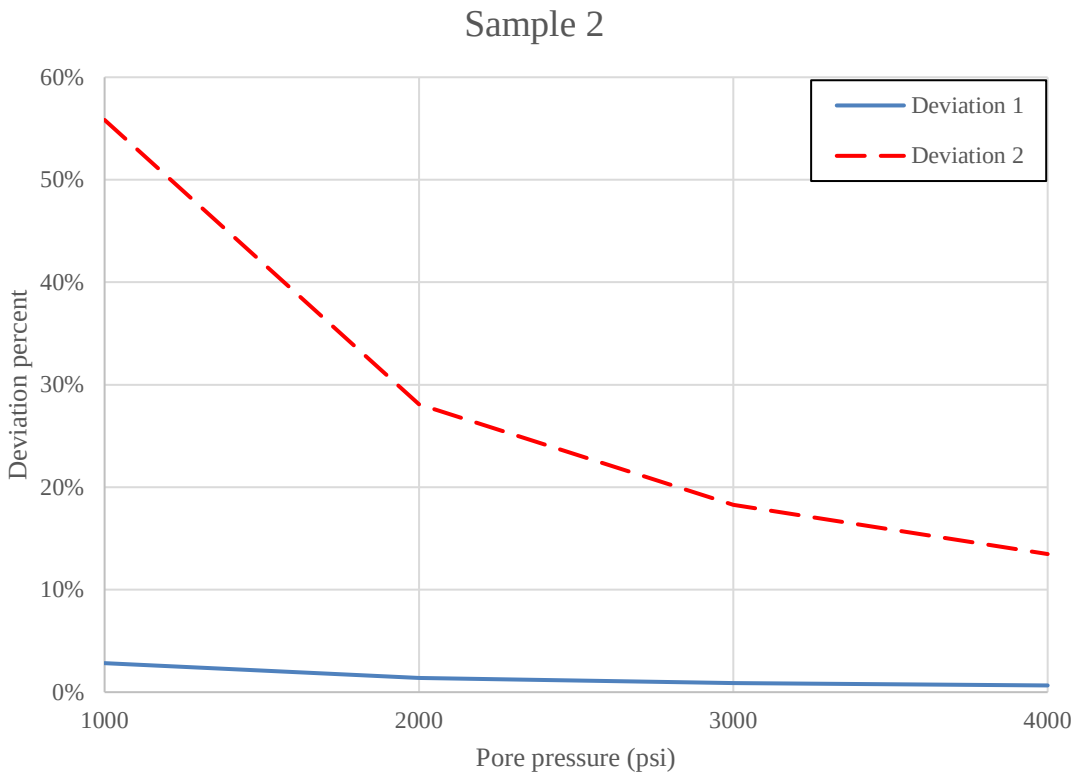

Figure 8: Sample 2 deviation percentage versus pore pressure.

Finally, the average density for twelve representative pore sizes was plotted for the four pressures used in this thesis on **Fig. 9**. As shown by Fig. 9, the average density for each pore size clearly follows a third order polynomial with R^2 values greater than 0.994. This would indicate that when calculating effective density, it is not necessary to generate density profiles and calculate average densities for each pore size so long as a sufficient number of average densities at the desired temperature and pressure, spanning the desired range, have already been found.

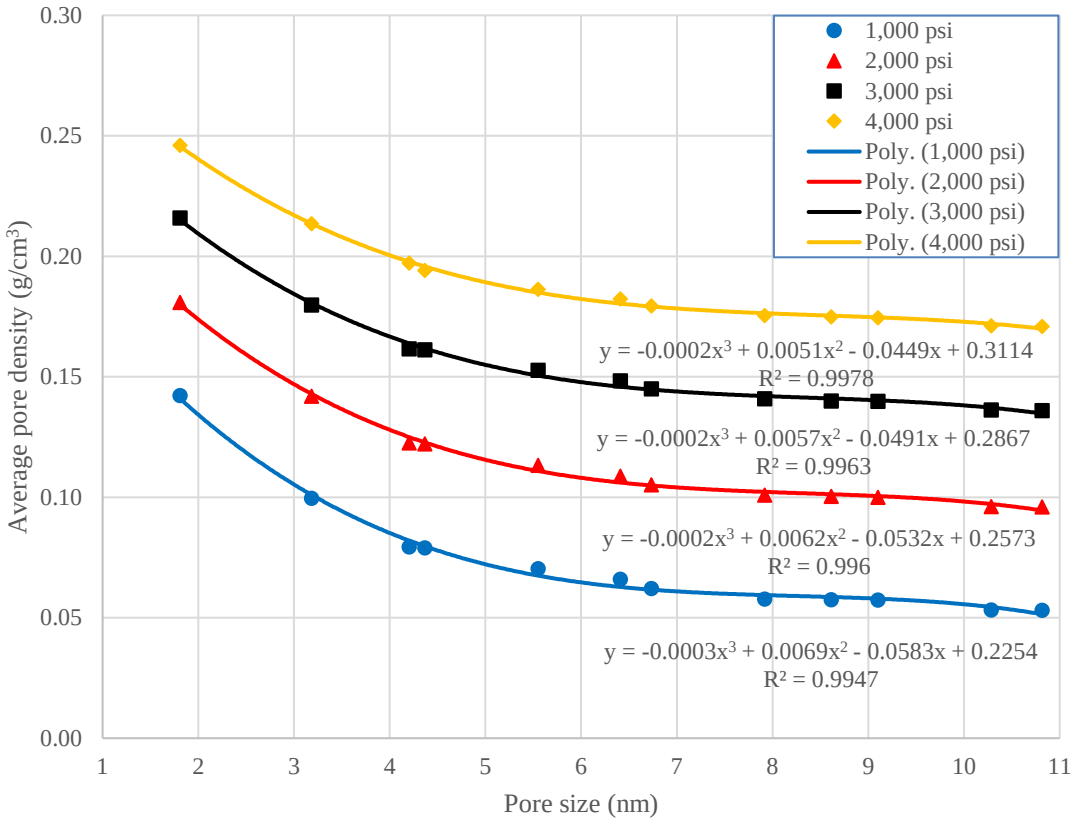

Figure 9: Average pore density as a function of pore size.

Chapter 5: Conclusions

This thesis has demonstrated the effect of a pore size on fluid densities in nanosize pores. The increase in fluid density in nanopores previously reported is shown and can be significant for pores less than 10 nm in diameter. However, what has also been shown is that the significance of this density increase on a sample is entirely dependent on the pore-body size distribution of the rock being studied. Furthermore, whether that distribution represents pore-body sizes or pore-throat sizes is also important.

For the two Barnett shale samples used in this thesis, it can be assumed that the effect of pore size on effective gas density is insignificant at pressures consistent with formation depth when calculating gas in place. This conclusion is reached assuming that the pore-body size distribution, not the pore-throat size distribution, best characterizes the pore geometry when calculating gas in place. For both samples, the error between pore-body and unconfined density was smaller than 1.0% when the pore pressure is greater than or equal to 3,000 psia. Compared to the error generated using the pore-throat size distribution at the same pressures, as much as 18%, we see the importance in specifying pore-body or pore-throat sizes when reporting data.

These numerical results are only valid for shales with similar properties as the Barnett shales used here, but they have important qualitative implications for developing a realistic reservoir model for shale formations. Reservoir simulators that use pore-throat size distributions to account for the presence of nanosize confinement overestimate effective density.

Substitution of pore-throat size for pore-body size will also impact gas-in-place estimates for gas shale reservoirs. Because the pore-throat size data clearly produces density values greater than those actually present in shale formations, gas-in-place estimates using pore-throat data will be overoptimistic. Ultimate recovery values will correspondingly be overoptimistic and projects expected to be profitable may end up generating unexpected losses for natural gas producers.

References

Ambrose, R.J., Hartman, R.C., Diaz-Campos, M. et al. 2012. Shale Gas-in-Place Calculations Part 1: New Pore-Scale Considerations. *SPE J* **17** (1), 219-229. https://doi.org/10.2118/131772-PA

Barbosa, G.D., Travalloni, L., Castier, M. et al. 2016. Extending an equation of state to confined fluids with basis on molecular simulations. *Chemical Engineering Science* **153** (22 October), 212-220. https://doi.org/10.1016/j.ces.2016.07.033

Bryant, S. L., Mellor, D. W. and Cade, C. A. 1993. Physically representative network models of transport in porous media. *AIChE J*. **39** (3), 387–396. https://doi.org/10.1002/aic.690390303

Chareonsuppanimit, P., Mohammad, S.A., Robinson Jr., R.L. et al. 2012. High-pressure adsorption of gases on shales: Measurements and modeling. *International Journal of Coal Geology* **95**, 34-46. https://doi.org/10.1016/j.coal.2012.02.005

Chen, J.H., Wong, D.S.H., Tan, C.S. et al. 1997. Adsorption and desorption of carbon dioxide onto and from activated carbon at high pressures. *Ind. Eng. Chem. Res.* **36** (7), 2808-2815.

Comisky, J.T., Santiago, M., McCollom, B. et al. 2011. Sample Size Effects on the Application of Mercury Injection Capillary Pressure for Determining the Storage Capacity of Tight Gas and Oil Shales. Presented at the Canadian Unconventional Resources Conference. Calgary, Alberta, 15-17 November SPE-149432-MS. http://dx.doi.org/10.2118/149432-MS

Danesh, A. 1998. *PVT and Phase Behavior of Petroleum Reservoir Fluids*, third edition. Boston: Elsevier Science

Denney, D. 2012. Shale-Gas Reserves Estimation: Multiple Decline-Curve-Analysis Models. *J Pet Technol* **64** (11), 144-148. http://dx.doi.org/10.2118/1112-0144-JPT

Didar, B.R. and Akkutlu, I.Y. 2013. Pore-size Dependence of Fluid Phase Behior and Properties in Organic-Rich Shale Reservoirs. Presented at the SPE International Symposium on Oilfield Chemisty. The Woodlands, Texas, 8-10 April SPE-164099-MS. http://dx.doi.org/10.2118/164099-MS

Dong, X., Lui, H., Hou, J. et al. 2016. Phase Equilibria of Confined Fluids in Nanopores of Tight and Shale Rocks Considering the Effect of Capillary Pressure and Adsorption Film. *Ind. Eng. Chem. Res*. **55** (3), 798-811. http://dx.doi.org/10.1021/acs.iecr.5b04276

EIA. 2017. Where Our Natural Gas Comes From. (10 January 2017 revision), https://www.eia.gov/energyexplained/index.cfm?page=natural_gas_where (accessed 20 April 2017).

Fatt, I. 1956. The Network Model of Porous Media. *Petroleum Transactions, AIME* **207**, 144-181.

Giaya, A. and Thompson, R.W. 2002. Water confined in cylindrical micropores. *The Journal of Chemical Physics* **117** (7), 3464-3475. http://dx.doi.org/10.1063/1.1494419

Hickey, J.J., and Henk, B. 2007. Lithofacies Summery of the Mississippian Barnett Shale, Mitchell 2 T.P. Sims well, Wise County, Texas. *AAPG Bulletin* **91** (4), 437-443. https://doi.org/10.1306/12040606053

Holovko, M., and Dong, W. 2009. A Highly Accurate and Analytic Equation of State for a Hard Sphere Fluid in Random Porous Media. *J. Phys. Chem. B* **113** (18), 6360-6365. https://doi.org/10.1021/jp809706n

Jiang, C., Bryant, S. and Daigle, H. 2015. A Bundle of Short Conduits Model of the Pore Structure of Gas Shale. Presented at the Unconventional Resources Technology Conference. San Antonio, Texas, 20-22 July URTEC-2169349-MS. https://doi.org/10.15530/URTEC-2015-2169349

Kuila, U. and Prasad, M. 2013. Specific Surface Area and Pore-size Distribution in Clays and Shales. *Geophysical Prospecting* **61** (1), 341–362. https://doi.org/10.1111/1365-2478.12028

Ma, Y. and Jamili, A. 2016. Modeling the density profiles and adsorption of pure and mixture hydrocarbons in shales. *Journal of Unconventional Oil and Gas Resources* **14**, (June) 128-138. https://doi.org/10.1016/j.juogr.2016.03.003

Mohammad, S.A., Chen, J.S., Robinson Jr., R.L. et al. 2009. Generalized Simplified Local-Density/Peng-Robinson Model for Adsorption of Pure and Mixed Gases on Coals. *Energy Fuels* **23** (12), 6259-6271. https://doi.org/10.1021/ef900642j

Montgomery, S.L., Jarvie, D.M., Bower, K.A. et al. 2005. Mississippian Barnett Shale, Fort Worth basin, north-central Texas: Gas-shale play with multi-trillion cubic foot potential. *AAPG Bulletin* **89 (**2), 155-175. http://dx.doi.org/10.1306/09170404042

Mosher, K., He, J., Liu, Y. et al. 2013. Molecular simulation of methane adsorption in micro- and mesoporous carbons with applications to coal and gas shale systems. *International Journal of Coal Geology* **109-110**, 36-44. https://doi.org/10.1016/j.coal.2013.01.001

Purcell, W. R. 1949. Capillary Pressures - Their Measurement Using Mercury and the Calculation of Permeability Therefrom. *J Pet Technol* **1** (2), 39-48. http://dx.doi.org/10.2118/949039-G

Rangarajan, B., Lira, C. T. and Subramanian, R. 1995. Simplified local density model for adsorption over large pressure ranges. *AIChE J*, **41** (4), 838–845. http://dx.doi.org/10.1002/aic.690410411

Sakhaee-Pour, A. and Bryant, S.L. 2015. Pore Structure of Shale. *Fuel* **143**, 467-475. https://doi.org/10.1016/j.fuel.2014.11.053

Schoen, M., and Diestler, D. 1998. Analytical Treatment of a Simple Fluid in a Slit-pore. *The Journal of Chemical Physics*. **109** (13), 5596-5606. http://aip.scitation.org/doi/abs/10.1063/1.477177

Shahamat, M. S., and Clarkson, C. R. 2017. Multi-Well, Multi-Phase Flowing Material Balance. Presented at the SPE Unconventional Resources Conference, Calgary, Alberta, 15-16 February. SPE-185052-MS. http://dx.doi.org/10.2118/185052-MS

Tinni, A., Odusina, E. Sulucamain, I. et al. 2014. NMR Response of Brine, Oil, and Methane in Organic Rich Shales. Presented at the SPE Unconventional Resources Conference, The Woodlands, Texas, 1-3 April. SPE-168971-MS. http://dx.doi.org/10.2118/168971-MS

Travalloni, L., Castier, M., Tavares, F., and Sandler, S. 2010. Thermodynamic Modeling of Confined Fluids Using an Extension of the Generalized van der Waals Theory. *Chemical Engineering Science*. **65** (10), 3088-3099 http://doi.org/10.1016/j.ces.2010.01.032

Travalloni, L., Castier, M., Tavares, F. 2014. Phase equilibrium of fluids confined in porous media from an extended Peng-Robinson equation of state. *Fluid Phase Equilibria* **362** (2014), 335-341. https://doi.org/10.1016/j.fluid.2013.10.049

Washburn, E.W. 1921. The Dynamics of Capillary Flow. *Phys. Rev.* **17** (3), 273-283.

Webb, P.A. 2001. An Introduction to the Physical Characterization of Materials by Mercury Intrusion Porosimetry with Emphasis on Reduction and Presentation of Experimental Data. Micromeritics, http://www.micromeritics.com/pdf/app_articles/mercury_paper.pdf (accessed 20 April 2017).

Xiaohu D., Huiqing L., Jirui H., et al. 2016. Phase Equilibria of Confined Fluids in Nanopores of Tight and Shale Rocks Considering the Effect of Capillary Pressure and Adsorption Film. *Industrial & Engineering Chemistry Research **55*** (3), 798-811. http://dx.doi.org/10.1021/acs.iecr.5b04276

Zapata, Y. and Sakhaee-Pour, A. 2016. Model adsorption-desorption hysteresis in shales: Acyclic pore model. *Fuel* **181**, 557-565. https://doi.org/10.1016/j.fuel.2016.05.002

Zarragoicoechea, G. and Kuz, V. 2002. Van der Waals Equation of State for a Fluid in a Nanopore. *Phys. Rev. E.* **65** (2), 021110-1-021110-4. http://dx.doi.org/10.1103/PhysRevE.65.021110

Zarragoicoechea, G. and Kuz, V. 2004. Critical Shift of a Confined Fluid in a Nanopore. *Fluid Phase Equilibria*. **220** (1), 7-9. http://doi.org/10.1016/j.fluid.2004.02.014

Zhu, H. Y., Ni, L. A., and G. Q. Lu. 1999. Pore-Size-Dependent Equation of State for Multilayer Adsorption in Cylindrical Mesopores. *Langmuir* **15** (10), 3632-3641. http://dx.doi.org/10.1021/la981515v